Am J Transl Res 2020;12(6):2473-2487
www.ajtr.org /ISSN:1943-8141/AJTR0104964

Original Article

Effects of fluorinated porcine hydroxyapatite on lateral ridge augmentation: an experimental study in the canine mandible

Yuanxiang Liu*, Chengwu Liu*, Ruoxuan Huang, Kaidi Chen, Baoxin Huang, Quan Liu, Zhuofan Chen, Zhipeng Li

*Guanghua School of Stomatology, Hospital of Stomatology, Sun Yat-sen University, Guangdong Provincial Key Laboratory of Stomatology, Guangzhou, China. *Co-first authors.*

Received November 15, 2019; Accepted May 18, 2020; Epub June 15, 2020; Published June 30, 2020

Abstract: Purpose: The aim of this study was to evaluate the effects of porcine hydroxyapatite (PHA) and fluorinated porcine hydroxyapatite (FPHA) applied concomitantly with collagen membranes (CMs) on bone regeneration in mandibular lateral ridge defects. Materials and methods: Mandibular third premolar to second molar were extracted bilaterally in six male beagle dogs. After 8 weeks of healing, six standardized box-shaped defects were bilaterally created at the buccal aspect of the mandibles and randomly allocated in a split-mouth design to the (i) PHA, (ii) FPHA or (iii) blank group and covered with CMs. After 12 weeks, biopsies of the defects were obtained for micro-computed tomography (micro-CT) evaluation and histological analysis. Results: Both FPHA and PHA promoted new bone formation and showed a better ridge width maintenance capacity than the blank control treatment. The micro-CT evaluation showed that the bone volume fraction (BV/TV) in the FPHA group was significantly higher than that in the PHA group. The trabecular number (Tb.N) in the FPHA group was significantly higher than that in the blank group. Histomorphometric analysis revealed a significantly larger area and higher ratio of newly formed bone in the FPHA group than those in the PHA group. The ratio of non-mineralized tissue in the FPHA group was significantly lower than that in the PHA group. No significant difference in the amount of residual materials was found between the FPHA and PHA groups. Conclusions: FPHA achieved better ridge width maintenance and bone regeneration outcomes than PHA as a bone substitute in lateral ridge augmentation.

Keywords: Animal experiments, bone substitutes, porcine hydroxyapatite, fluoride ion, lateral ridge augmentation, guided bone regeneration

Introduction

Dental trauma, periodontitis, and periapical infection are common causes of tooth loss and are often accompanied by destruction and resorption of the alveolar bone, which limits the placement of dental implants [1, 2]. During the past few decades, guided bone regeneration (GBR), an effective approach, has been used to reconstruct bone defects either before or during the placement of dental implants. The principle of GBR is to use a barrier membrane to isolate the bone augmentation region from epithelial and connective tissues and thus prevent the rapid proliferation of epithelial cells by preemptively occupying the augmented area while allowing the proliferation and osteoblastic differentiation of bone-forming cells to promote bone formation and maturation [3, 4]. The stability of the bone regeneration space is one of the critical factors influencing the outcome of GBR. To ensure the stability of the space, bone graft materials are commonly used in conjunction with barrier membranes in GBR procedures [5]. Bone graft materials with certain mechanical strength can also help to resist external pressure and improve the stability of the bone regeneration space [6, 7]. Furthermore, the materials are osteoconductive and can be used as a scaffold for the growth of bone-forming cells and to promote bone formation [8]. Calcium phosphate-based bone graft materials are commonly used bone substitutes in GBR in the dental field, and hydroxyapatite (HA) and tri-

calcium phosphate (TCP) have been the most widely studied materials [9, 10].

HA, the main inorganic component in human bones, has been demonstrated to show superior osteoconductivity when used as a bone substitute [10, 11]. HA can be divided into biological HA and chemical synthetic HA. Biological HA is mainly derived from animal bones and is highly similar to human bone in both structure and chemical composition. Accordingly, biological HA has been the most widely used bone substitute in clinical practice [12]. Biological HA originates from a variety of sources, including bovines, deer, and coral [13]. Deproteinized bovine bone mineral is one of the most commonly used biological HAs in dentistry [5]. However, compared with materials of bovine origin, porcine bone, which bears the closest resemblance to human bone in terms of microstructure and chemical composition, is a better alternative source for preparing biological HA [13]. In addition, porcine bone-derived hydroxyapatite (PHA) has shown outstanding biocompatibility and superior osteoconductivity as a bone substitute for bone regeneration, and most PHA has demonstrated favorable bone healing performance during augmentation of the alveolar bone and maxillary sinus [14-16]. However, because biological HA has no osteoinductivity, further modifications of this material are needed to improve its biological performance.

Trace element ions can significantly improve the physicochemical and biological properties of HA. Therefore, trace element substitution into HA has been considered an effective method for HA modification. For example, zinc and strontium substitution can stimulate osteoblast activity while inhibiting osteoclast function [17, 18]. In addition, magnesium and silicate can promote early angiogenesis, which plays an important role in bone remodeling [19, 20]. Similarly, fluorine is an essential trace element in bone tissue, and an appropriate concentration of fluorine ions can promote the proliferation and differentiation of osteoblasts [21, 22]. Furthermore, fluorine can stimulate bone formation and increase bone mass without prior bone resorption [23]. In our previous study, fluorine was incorporated into PHA through a novel thermal chemical treatment to prepare fluorinated porcine bone-derived hydroxyapatite (FPHA) [13]. Compared with PHA, the appropriate level of fluoridation of FPHA stimulated osteogenic differentiation of bone-forming cells in vitro and promoted bone regeneration in rat and rabbit calvaria defects in vivo [14-16], indicating that FPHA may be a promising bone substitute material for bone defect regeneration. Before clinical application of the novel FPHA bone graft material, the effects of fluoridation of PHA on the repair of bone defects require further verification.

The aim of the present study was to evaluate the effects of PHA and FPHA materials on lateral ridge augmentation at acute-type defects in canine mandibles using the documented GBR procedure. The hypothesis was that fluoridation of PHA can promote bone regeneration in canine mandible defects.

Materials and methods

Preparation of PHA and FPHA

Preparation of FPHA consists of two steps as established in our previous study: preparation of PHA and substitution of fluorine. Briefly, macroscopic impurities were removed from porcine bones after boiling in distilled water at 100°C for 4 hours. Subsequently, the bones were soaked in 30% hydrogen peroxide for 24 hours and then anhydrous ethanol for 48 hours to remove the partial fat and protein. Next, the bones were cut into regular blocks with a diameter of 8 mm and a thickness of 3 mm. The bone blocks were calcinated at 800°C for 2 hours to eliminate organic components, and PHA blocks were obtained. Next, the PHA blocks were immersed in a 0.25 M NaF aqueous solution for 24 hours and then calcinated again at 700°C for 3 hours to obtain FPHA blocks. Finally, both the PHA and FPHA bone blocks were ground into granules with a diameter ranging from 0.25-1 mm and sterilized for use.

Animals

Six beagle dogs (aged 17-20 months and weighing 12-15 kg) were used in the study. All animals exhibited fully erupted permanent dentition. The animals were kept in separate cages, received food (a soft-food diet during the experimental period) twice daily, and had ad libitum access to water. The animal selection, management, and surgery protocols were carried out in

strict accordance with the Institutional Animal Care and Use Committee (IACUC) of Sun Yat-sen University and were approved by the Animal Ethical and Welfare Committee of Sun Yat-sen University (IACUC-DD-17-1206). The experiments started after an adaptation period of 2 weeks.

Study design and randomization

The animal surgery in the study was divided into two phases. In the first surgical phase, the mandibular 3rd and 4th premolars, as well as the 1st and 2nd molars (P3-M2), were extracted bilaterally in each dog. After 8 weeks of healing, in the second surgical phase, three standardized box-shaped defects were surgically created at the buccal aspect of the alveolar ridge bilaterally in the mandible. The box-shaped defects were randomly allocated in a split-mouth design to the (i) PHA, (ii) FPHA or (iii) blank control group. Randomization was performed according to a computer-generated protocol (Excels, Microsoft, USA) and accounted for a potential difference between anterior and posterior defect characteristics. The animals were sacrificed after a healing period of 12 weeks after surgical phase 2.

Surgical phase 1

General anesthesia was induced by an intravenous injection of ketamine (10 mg/kg) and diazepam (0.3 mg/kg) followed by placement of an endotracheal tube. General anesthesia was maintained with isoflurane (approximately 0.5%-4%) in oxygen. A fentanyl patch (50 μg/hour) was applied to the skin to provide analgesia for up to 72 hours. Additionally, prophylactic penicillin G (300,000 U, Pen-B®, Pfizer Inc., Lee's Summit, USA) was administered during and after each surgical phase every 48 hours for 10 days. During the surgery, P3-M2 were carefully extracted bilaterally from the mandible after reflection of the mucoperiosteal flaps and tooth separation (**Figure 1A**, **1B**). After wound closure by tension-free suture, the tooth extraction sites were allowed to heal for 8 weeks.

Surgical phase 2

Bilateral alveolar crest incisions were made, and the mucoperiosteal flaps were reflected to expose the buccal plate of the alveolar bone. Then, three standardized box-type defects (9 mm in height from the crestal bone, 5 mm in depth from the surface of the buccal bone, and 10 mm in width mesiodistally) were prepared in the buccal bone with a straight fissure carbide bur. The distance between each pair of defects was greater than 5 mm to ensure the integrity of the bone walls. The lingual bone plate in each defect was left intact. The defect size was accurately measured using a periodontal probe (Hu-Friedy, USA). A total of six defects were prepared in each dog's mandible. All osteotomy surgeries were performed under copious irrigation with sterile 0.9% physiological saline. After blood infiltration in the bone grafting bed was confirmed, the defect sites for lateral ridge augmentation in both mandibles were randomly augmented with (i) PHA, (ii) FPHA or (iii) Blank. The defect sites in all groups were covered by a native type I/III collagen membrane (CM, Bio-Gide®, Geistlich, Switzerland). The CM was trimmed and adapted over the entire defect area to cover 2 mm of the surrounding alveolar bone. No screws or pins were used to stabilize the membranes. Following periosteal-releasing incisions, the mucoperiosteal flaps were repositioned coronally and fixed with tension-free suture (**Figure 1C-G**).

Retrieval of specimens

The animals were sacrificed after a healing period of 12 weeks. Euthanasia was performed with an overdose of 4% pentobarbital sodium (120 mg/kg/i.v.). Subsequently, oral tissues were fixed by perfusion with 10% neutral-buffered formalin administered through the carotid arteries. The mandibles were extracted, and the muscles around the mandibles were removed. All specimens were fixed in 10% neutral-buffered formalin solution for 10 days.

Micro-computed tomography (micro-CT) scan

The specimens were dissected into small blocks, and each block contained one defect site. Micro-CT scanning was performed on all specimens. Each mandible sample was positioned in a suitable scanning tube. The micro-CT scanner (SCANCO μCT50, Switzerland) was operated with a resolution of 20 μm, a source voltage of 70 kV, and a current of 200 μA. Three-dimensional images were obtained and reconstructed using the supporting software from the scanner. The volume of interest (VOI)

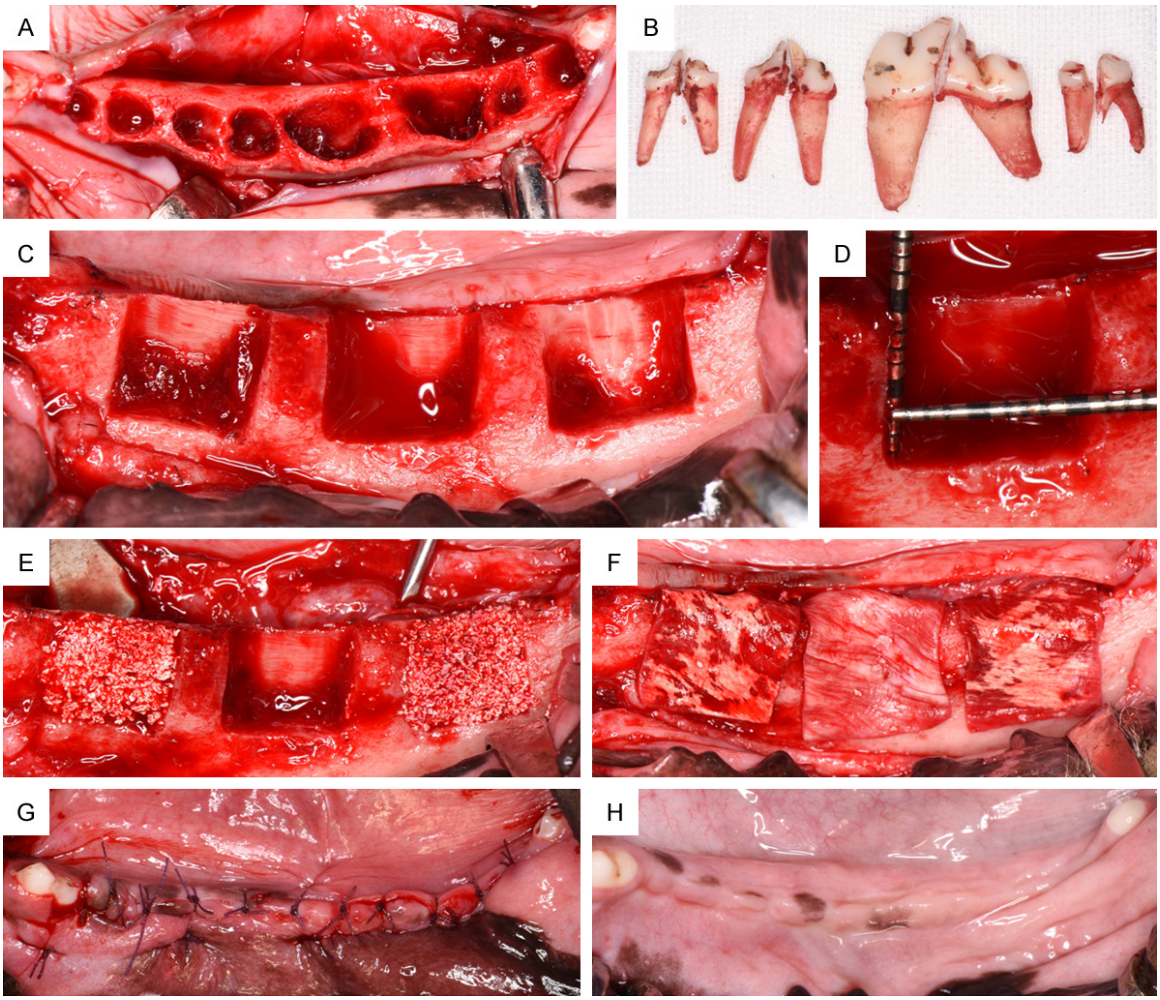

Figure 1. Schematic description of the animal experimental model. A. Extraction sockets of the third and fourth premolars and first and second molars (P3-M2). B. P3, P4, M1 and M2 after tooth separation and extraction. C. Eight weeks after tooth extraction, three standardized box-type defects (9 mm in height from the crestal bone, 5 mm in depth from the surface of the buccal bone, and 10 mm in width mesiodistally) were bilaterally created at the buccal aspect of each hemimandible (n=6 defects per animal). D. Clinical measurement of the defect size with a periodontal probe before regenerative surgery. E. Augmentation treatment for each defect from left to right: PHA; blank; and FPHA. Graft materials were applied to homogeneously fill the complete defect area. F. All sites were protected by a native collagen membrane covering 2 mm of the surrounding alveolar bone. G. The mucoperisteal flaps were advanced to ensure a tension-free submerged healing procedure. H. The augmented sites were allowed to heal for 12 weeks; healing in the mandible was uneventful.

was located in the central region of each defect with a width of 5 mm mesiodistally, which was delimited using the line of demarcation between the parent bone and the newly formed bone (NB) for the internal and inferior borders of the bone defect area. The buccal border of the VOI was defined by the boundary of hard and soft tissues (**Figure 2A-F**). The bone volume fraction (BV/TV), bone trabecular thickness (Tb.Th), bone trabecular number (Tb.N), and bone trabecular separation degree (Tb.Sp) of the VOI in each group were measured using the scanner software.

Histological preparation

All specimens were dehydrated using a gradient ethanol series, cleared in xylene, and infiltrated and embedded in a methylmethacrylate (MMA, Technovit 9100 NEU, Heraeus Kulzer, Germany) and dibutylphthalate mixture for nondecalcified sectioning. After the specimens were completely polymerized, serial sections (Exakts®, Apparatebau, Germany) were prepared from the central region of each defect site in the labiolingual direction. Ten sections with a thickness of approximately 500 μm were

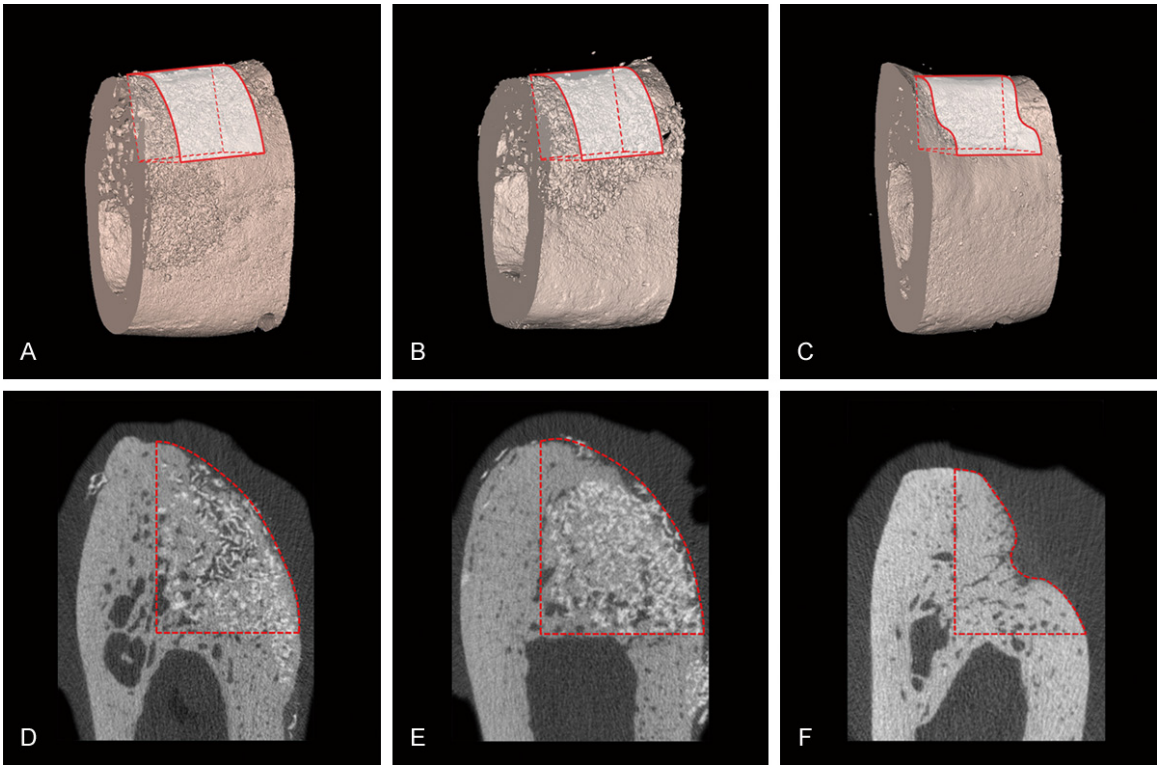

Figure 2. Micro-CT results of 3D and corresponding 2D representative images of the defect sites in the three groups at 12 weeks. (A-C) 3D reconstruction. (D-F) 2D section. The original contour of the ridge at the defect sites was successfully maintained by PHA (A, D) and FPHA (B, E). The contour of the ridge at the defect sites was obviously collapsed in the blank group (C, F). The residual PHA (D) and FPHA (E) particles showed the highest grey values due to their high density and could be distinguished from newly formed bone in the CT sections. Both PHA (D) and FPHA (E) particles were surrounded by newly formed bone.

obtained from each specimen. Next, all sections were glued to opaque plexiglass using acrylic cement and sanded to an ultimate thickness of approximately 50 μm. After final polishing, sections representing the central regions of the defect areas were ready for histomorphometric analysis (McNeal's tetrachrome staining solution, basic fuchsine and toluidine blue O).

Histological analysis

Histomorphological images were obtained by a stereomicroscope (KL 1500, Leica Microsystems GmbH, Germany) and an Axioskop 40 microscope (Zeiss, Germany). The digital images were analyzed using Image-Pro Plus 6.0 software (Media Cybernetic, USA) at 10× magnification. All measurements were performed by two experienced examiners.

The following standard lines were marked on the images by one experienced investigator blinded to the experimental treatment of each stained section: the bottom of the defect (BD) and the highest point of the alveolar ridge of the defect (HD). The defect height (DH, mm) was measured from the HD to the BD, and the width of the ridge (WR, mm) after bone augmentation was measured at 0%, 25%, 50%, 75%, and 100% of the DH (**Figure 3A**).

The region of interest (ROI, mm^2) representing the bone augmented area was evaluated from the HD to the BD of the defect area. Within the ROI, the area and area ratio of the NB and non-mineralized tissue (NMT) and the amount of residual material (RM) were automatically calculated (mm^2, %, **Figure 3B**, **3C**).

Before the histomorphometric evaluation was formally started, the selected examiners and the analysis software were calibrated with a standard: the similarity level of repeated measurements was > 95% for each section.

Statistical analysis

Statistical analysis was performed using a commercially available software program (SPSS 22.0, SPSS Inc., USA). Continuous vari-

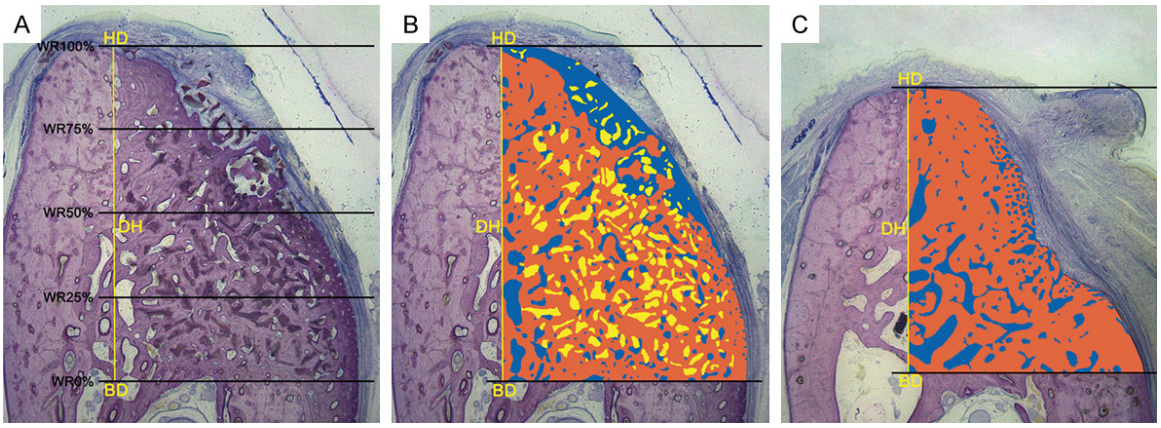

Figure 3. Methods of histomorphometric analysis. A. The following landmarks were identified in the stained sections: the bottom of the defect (BD) and the highest point of the alveolar ridge of the defect (HD). The defect height (DH, mm) was measured from the HD to the BD, and the width of the newly formed ridge (WR, mm) was measured at 0%, 25%, 50%, 75%, and 100% of the DH. B and C. The colored area, measured from the BD to the HD, represents the region of interest (ROI) of the augmentation procedure. Within the ROI, the different colors represent different structures: Orange = new bone; blue = non-mineralized structures; and yellow = residual material. The area (mm^2) and proportion (%) of the different structures were calculated (McNeal stained, original magnification 10×).

ables were described as the mean and standard deviation (SD) or the median and interquartile range (IQR) according to their distributions. The data was examined with the Kolmogorov-Smirnov test for normal distribution, and variance homogeneity was tested by Levene's test.

In the micro-CT evaluation, the normality assumption was rejected for all the outcomes (the BV/TV, Tb.Th, Tb.N and Tb.Sp, $P < 0.10$). The values for the parameters are presented as the median and IQR. The Kruskal-Wallis rank test was used for all inter-group comparisons, and pairwise post hoc comparisons were performed using the Wilcoxon-Mann-Whitney test with Bonferroni-corrected *P* values. In the histomorphometric and alveolar ridge width evaluations, the assumption of normality was proven by *P* values > *0.10*. Therefore, the values for the parameters are presented as the mean ± SD. In addition, the results of Levene's test demonstrated variance homogeneity ($P > 0.10$). Thus, one-way analysis of variance (one-way ANOVA) was used for all inter-group comparisons, and post hoc comparisons were performed using Bonferroni-adjusted Student's t-tests. Since no material was used in the blank group, the independent-samples t-test was used to compare the size and proportion of RMs between the PHA and FPHA groups. Statistically significant differences were considered for *P* values < *0.05*.

Results

Postoperative healing was uneventful in all dogs. No complications, such as allergic reactions, infections or abscesses, were observed throughout the entire study period. Accordingly, a total of n=12 (PHA), n=12 (FPHA) and n=12 (blank) sites were included for the micro-CT and histological analyses.

Micro-CT evaluation

Regenerative new bone had formed at the defect sites in all groups by 12 weeks after surgical phase 2. Bone substitutes and new bone could be identified in the CT sections (**Figure 2D-F**). The granular bone substitutes were surrounded by NB, and the contours of the defect sites were supported by the PHA and FPHA materials. Compared with the PHA and FPHA groups, substantially more contour collapse was noted in the blank group. A 3D-CT image was reconstructed to observe the contour shape of each defect site (**Figure 2A-C**). A greater BV/TV, Tb.Th, and Tb.N corresponded to a more mature and steadier bone structure. In contrast, if the Tb.Sp was large, then the close and ordered arrangement of the 3D network and the bone structure were poor. The results of the Kruskal-Wallis rank test indicated that the differences in the BV/TV, Tb.N and Tb.Sp were significant ($P < 0.05$); thus, further post hoc comparisons were conducted (median,

Table 1. Micro-CT analysis results of the BV/TV, Tb.Th, Tb.N and Tb.Sp of the VOI for the different treatment groups: PHA, FPHA and blank (median, interquartile ranges)

Analyzed structures	Treatment groups		
	PHA	FPHA	Blank
BV/TV (%)	36.72, 9.39	41.97, 8.63*	65.06, 13.38*,#
Tb.N	3.20, 1.29	3.53, 0.49	2.67, 1.93#
Tb.Th	0.46, 0.18	0.40, 0.37	0.47, 0.12
Tb.Sp	0.33, 0.14	0.27, 0.14	0.67,0.51*,#

PHA: porcine hydroxyapatite, FPHA: fluorinated porcine hydroxyapatite, VOI: volume of interest, BV/TV: bone volume fraction, Tb.N: bone trabecular number, Tb.Th: bone trabecular thickness, Tb.Sp: bone trabecular separation degree. *: Compared with the PHA group, $P < 0.05$ using the Wilcoxon-Mann-Whitney test with Bonferroni correction. #: Compared with the FPHA group, $P < 0.05$ using the Wilcoxon-Mann-Whitney test with Bonferroni correction.

IQR). The FPHA group showed more new bone formation (BV/TV, 41.97, 8.63%) in the VOI than the PHA group (36.72, 9.39%). The Tb.N in the VOI in the FPHA group (3.53, 0.49) was significantly higher than that in the blank group (2.67, 1.93). No significant difference in Tb.Th was found among the three groups. The Tb.Sp in the VOI in the blank group (0.67, 0.51) was significantly higher than those in both the PHA (0.33, 0.14) and FPHA (0.27, 0.14) groups (**Table 1**).

Descriptive histology

At 12 weeks, histological observation revealed that the CMs ensured homogeneous stabilization of bone substitute materials in both the PHA and FPHA groups. Most sites grafted with bone substitutes showed a dome-shaped contour of the augmented alveolar crest, whereas most sites in the blank group revealed a collapsed contour at the buccal aspect (**Figure 4A-C**). Through McNeal staining, newly regenerated bone was stained with a deep pink color, while the parent bone was stained with a light pink color, which helped to clearly identify the border between the NB and the parent bone (**Figure 4A-C**).

In both the PHA and FPHA groups, granular bone substitutes integrated with native bone were clearly visible in the augmented areas (**Figure 5A**, **5B**). In the FPHA group, the mineralization of NB adjacent to the parent bone appeared to be more mature than that of bone far from the parent bone in the augmented area (**Figure 5C**, **5D**), indicating that the bone growth direction was from the parent bone to the center of the defect. Interestingly, the natural micropores on the material particles could also be observed (**Figure 5E**). The material particles, which were surrounded by newly formed lamellar bone, acted as a core of bone regeneration (**Figure 5A**, **5B**). The region above the BD was filled with NB surrounding integrated bone substitute particles and bone marrow. Most of the NB was mature and compact, and lamellar bone could be easily observed in the FPHA-grafted area (**Figure 5F**). A small amount of cell-rich and incompletely mineralized woven bone could be identified around the mature bone (**Figure 5D**), and a few multinucleated osteoclast-like cells were attached on the demineralized white seams on the bone substitutes (**Figure 5G**). Inside the ROI, many new blood vessels could be observed in the bone marrow. The growth of new bone and blood vessels could also be identified in the macropores of the materials (**Figure 5H**), indicating outstanding osteoconductivity of FPHA. Some grafted particles and NB with resorption lacunae and multinucleated osteoclast-like cells could be observed at the border of the augmented area adjacent to the fibrous connective tissue, which was blocked outside the augmented area (**Figure 5I**). Inflammatory cells were scarcely observed in the PHA and FPHA augmented area.

Histomorphometric evaluation

The one-way ANOVA results indicated that the differences in the ROIs, new bone and non-mineralized tissue were significant ($P < 0.05$); thus, further post hoc comparisons were conducted. The results of post hoc comparisons of the histological measurements are presented in **Table 2**. After 12 weeks, the mean ROI sizes in both the PHA and FPHA groups were significantly larger than that in the blank group. The area of new bone in the FPHA group (16.90±2.53 mm^2) was the highest among the three groups. The FPHA group also showed a higher proportion of new bone (40.92±4.79% versus 35.25±4.79%) and a lower proportion of non-mineralized tissue (31.72±4.00% versus 38.18±5.45%) than the PHA group, and these differences were statistically significant. The areas and proportions of RMs between the FPHA and PHA groups

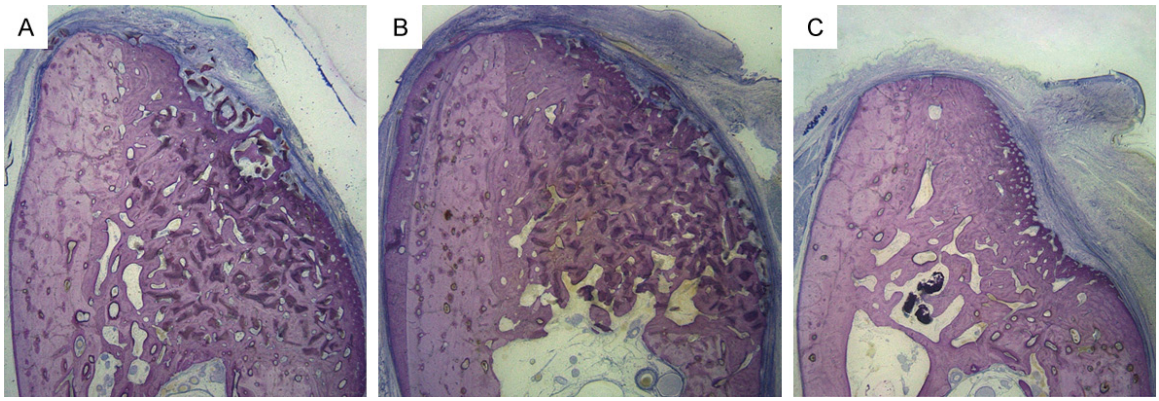

Figure 4. Representative histological low-magnification views of wound healing in the three groups at 12 weeks (McNeal stained, original magnification 10×). McNeal staining indicated a similar pattern of bone regeneration in both the PHA (A) and FPHA (B) groups. (A) PHA group: PHA particles were surrounded by newly formed bone, and the contour of the defect site was maintained. (B) FPHA group: FPHA particles were surrounded by newly formed bone, and ridge width maintenance was superior to that in the PHA site. (C) Blank group: At the blank site, a certain amount of newly formed bone and obvious collapse of the contour could be observed. In all sites in the three groups, the lateral boundary of the bone augmentation area was covered with fibrous connective tissue. The different stain colors represent different structures: Deep pink=newly formed bone; light pink = parent bone; and blue = fibrous connective tissue.

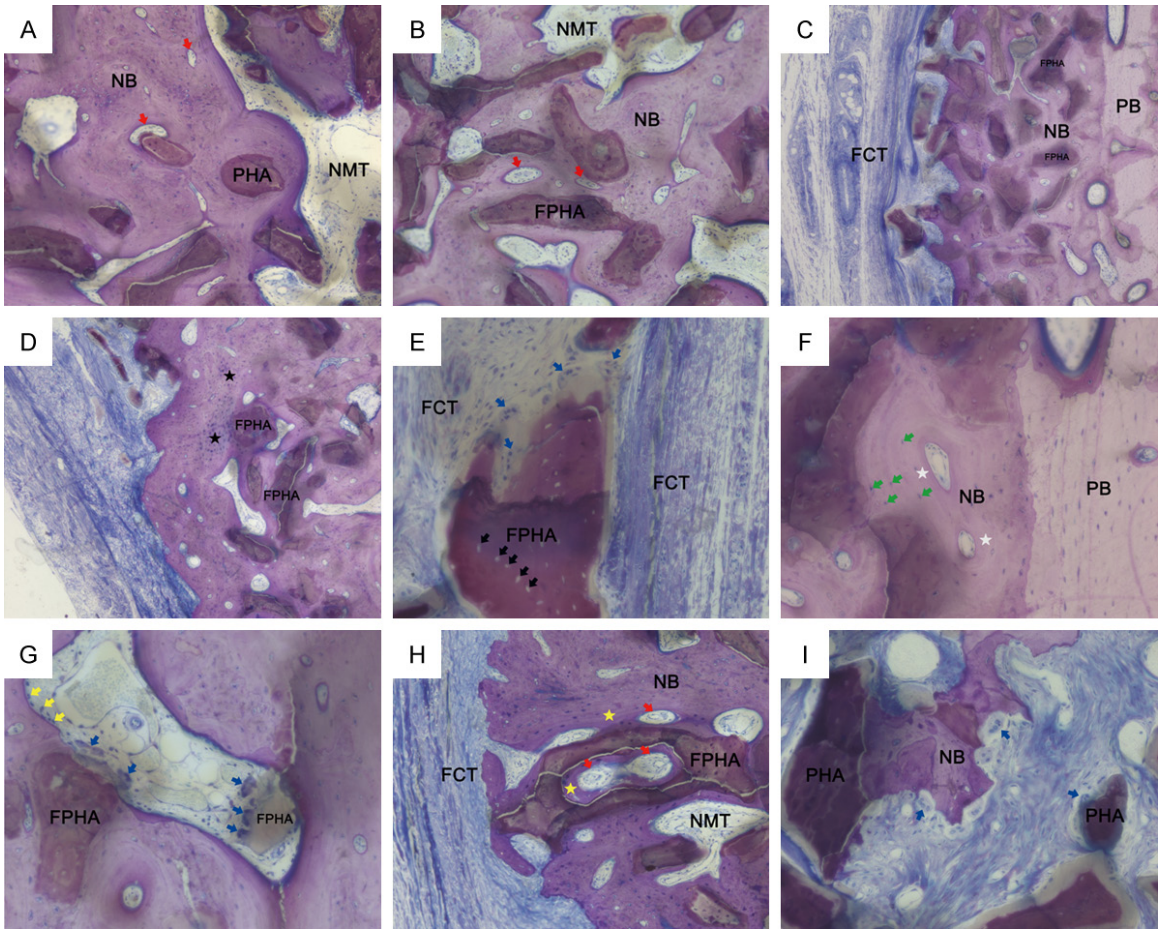

Figure 5. Representative histological high-magnification views of wound healing in the three groups at 12 weeks (McNeal stained). (A) FPHA and (B) PHA particles were integrated into newly formed bone (NB) with non-mineralized tissue (NMT) and blood vessel formation (red arrow) (original magnification 100×). (C) McNeal staining showing dif-

ferent stages of bone remodeling. Immature woven bone was observed in newly formed bone adjacent to the fibrous connective tissue (FCT). Mature lamellar bone was observed in the NB adjacent to the parent bone (PB) (original magnification 50×). (D) NB adjacent to FCT showing woven bone (black star) around grafted particles. (original magnification 50×). (E) FPHA particles with natural micropores (black arrow). Grafted particles encapsulated by FCT were observed with multinucleated osteoclast-like cells outside the NB area (original magnification 200×). (F) NB adjacent to PB showing lamellar bone with osteons (white star) and osteocytes within the lacunae of bone (green arrow) (original magnification 200×). (G) In the center of the augmented area, osteoblasts (yellow arrow) in the bone marrow were observed lining onto the NB. Resorption lacunae and multinucleated osteoclast-like cells (blue arrow) were observed at the demineralized surface of grafted particles (original magnification 200×). (H) NB (yellow star) and blood vessels growing into and around FPHA particles were observed in augmented areas (original magnification 100×). (I) Bone remodeling at the border of the augmented area adjacent to FCT. Grafted particles and NB surrounded by FCT were observed with resorption lacunae and multinucleated osteoclast-like cells (blue arrow) (original magnification 200×).

Table 2. Histomorphometric measurements of the size (mm^2) of the ROI and the proportion (%) area occupied by the new bone, RMs and NMT components for the different treatment groups: PHA, FPHA and blank (mean ± standard deviation)

Analyzed structures	Treatment groups					
	PHA		FPHA		Blank	
	mm^2	%	mm^2	%	mm^2	%
ROI	38.31±4.12	100	41.34±4.28	100	17.63±1.03*,#	100
New bone	13.52±2.50	35.25±4.79	16.90±2.53*	40.92±4.79*	11.18±1.39#	63.30±5.36*,#
Residual materials	10.12±1.46	26.57±3.94	11.30±2.27	27.36±4.76	/	/
Non-mineral. tissue	14.66±2.75	38.18±5.45	13.15±2.41	31.72±4.00*	6.45±0.88*,#	36.70±5.36

PHA: porcine hydroxyapatite, FPHA: fluorinated porcine hydroxyapatite, ROI: region of interest. *: Compared with the PHA group, $P < 0.05$ using Bonferroni-adjusted Student's t-tests. #: Compared with the FPHA group, $P < 0.05$ using Bonferroni-adjusted Student's t-tests. The independent-sample t-test was used for the size and proportion of the residual materials.

were comparable. No significant difference in the area of non-mineralized tissue was identified between the FPHA and PHA groups.

Alveolar ridge width evaluation

The DH and ridge width measurements at 100%, 75%, 50%, 25%, and 0% of the DH in the three groups are presented in **Table 3**. After 12 weeks of healing, both the PHA and FPHA groups showed significantly higher DHs and ridge width measurements at 100%, 75%, 50%, and 25% of the DH than the blank control group. Both the PHA and FPHA groups had comparable mean DH values and WR values at 100%, 25% and 0% of the DH. However, the mean WR values at 75% (5.36±0.50 mm versus 4.30±0.40 mm) and 50% (6.29±0.92 mm versus 5.28±0.74 mm) of the DH were significantly higher in the FPHA group than in the PHA group.

Discussion

PHA is a favorable biomaterial for bone tissue engineering due to its biocompatibility and osteoconductivity. In particular, this material is similar to natural bone in composition and microstructure and provides an excellent scaffold for the formation of new bone [24, 25]. The results of our previous study demonstrated that PHA had excellent osteoconductivity and biodegradability and could promote bone repair in rat calvarial defects [16, 26]. In the present study, the superior osteoconductivity of PHA was also confirmed in lateral ridge augmentation in canine mandibles. In the PHA-grafted area, NB and blood vessels grew into and around the material particles with natural macropores and micropores. FPHA retained the porous structure and osteoconductivity of PHA. In addition, fluorine ions can be constantly released from FPHA [14, 16]. Fluorine is an essential trace element involved in bone remodeling, and an appropriate concentration of fluorine ions plays an important role in the promotion of osteogenesis [27]. However, an excessive concentration of fluorine ions is cytotoxic and induces apoptosis [21, 22]. Our previous studies demonstrated that FPHA with a fluorine atomic percentage ranging from 1.50 to 3.12 can promote the osteoblastic differentiation of MG63 cells better than FPHA with a

Table 3. Histomorphometric measurements of the height (mm) and the mean WR (mm) measured at 0%, 25%, 50%, 75%, and 100% of the DH (mm) of the ROI for the different treatment groups: PHA, FPHA and blank (mean ± standard deviation)

Linear measurements, mm	Analyzed structures	Treatment groups		
		PHA	FPHA	Blank
Height		7.03±0.62	6.97±0.60	5.87±0.55*,#
100% level	New mineralized tissue with material	2.13±1.03	2.61±1.18	1.04±0.55#
	Non-mineralized tissue with material	0.42±0.25	0.35±0.28	0
	Total ROI	2.55±1.10	2.96±1.16	1.04±0.55*,#
75% level	New mineralized tissue with material	3.71±0.81	4.91±0.57*	1.97±0.33*,#
	Non mineralized tissue with material	0.59±0.62	0.45±0.34	0
	Total ROI	4.30±0.40	5.36±0.50*	1.97±0.33*,#
50% level	New mineralized tissue with material	4.85±0.84	5.63±0.67	2.54±0.51*#
	Non mineralized tissue with material	0.43±0.51	0.67±0.45	0
	Total ROI	5.28±0.74	6.29±0.92*	2.54±0.51*,#
25% level	New mineralized tissue with material	5.52±0.54	5.81±0.76	3.80±0.71*,#
	Non mineralized tissue with material	0.31±0.27	0.49±0.21	0
	Total ROI	5.83±0.63	6.29±0.71	3.80±0.71*,#
0% level	New mineralized tissue with material	5.39±0.39	5.67±0.83	5.26±0.39
	Non mineralized tissue with material	0.29±0.33	0.28±0.23	0
	Total ROI	5.68±0.46	5.95±0.71	5.26±0.39#

PHA: porcine hydroxyapatite, FPHA: fluorinated porcine hydroxyapatite, ROI: region of interest, WR: width of the ridge, DH: defect height. *: Compared with the PHA group, $P < 0.05$ using Bonferroni-adjusted Student's t-tests. #: Compared with the FPHA group, $P < 0.05$ using Bonferroni-adjusted Student's t-tests.

higher fluorine dose [14]. Another study showed that an FPHA extract with a fluorine ion concentration of 0.89±0.11 mg/L promoted the osteoblastic differentiation ability of rBMSCs better than a PHA extract [16, 22]. In our previous study, we demonstrated that FPHA can enable sustained release of not only fluorine ions but also some endogenous ions (e.g., magnesium and calcium) in the peripheral microenvironment, which led to a superior osteogenic response of rBMSCs in vitro and enhanced new bone formation in rat calvarial defects in vivo. On one hand, fluorine ions released from FPHA have been proven to significantly increase the osteogenic-related gene expression of ALP, Runx2, and OCN in vitro. On the other hand, a microenvironment with other released endogenous ions driven by fluoride incorporation may contribute to activation of Wnt/β-catenin signaling, which may directly enhance bone formation [16, 26]. These conclusions from the above studies might explain the underlying mechanism of FPHA enhancing bone regeneration in canine mandibles in the present study.

Numerous studies have suggested that the microstructural characteristics of NB can be demonstrated by micro-CT through 3D reconstruction and bone trabecular analysis, which provide a quick, accurate, nondestructive, and efficient evaluation method for basic and clinical research on bone regeneration [28, 29]. The bone microstructure plays an important role in the quality of NB after the GBR procedure. Therefore, micro-CT was adopted in the present study. BV/TV, Tb.Th, Tb.N and Tb.Sp are the most decisive parameters for evaluating trabecular bone microstructure and evaluating the microarchitecture of new bone [28, 30]. These parameters play a significant role in alveolar bone mechanical properties, which are crucial for the long-term success of bone augmentation. Similar parameters from micro-CT scans were reported in this study on trabecular bone for all three groups. The results of the micro-CT evaluation, which objectively reflect the actual biomechanical properties of new bone [31], indicated that the trabecular bone in the NB of the FPHA group was more regularly and closely arranged than that in the PHA group. As we mentioned above, micro-CT scans can evaluate the bone regeneration outcome of an entire defect site macroscopically, especially with the use of 3D measurements, which rep-

resent the most significant advantage of this method compared with histomorphometric analysis. However, accurately distinguishing between bone graft materials and regenerated new bone based on micro-CT evaluation is difficult. In contrast, histomorphometric analysis can accurately measure the areas and proportions of different structures. Therefore, in this study, these two methods were combined to comprehensively evaluate the bone regeneration capacity of the PHA and FPHA materials.

The osteoconductivity of FPHA promoted the maturation of NB, and the appearance of osteogenic-associated cells in the ROIs confirmed the effective bone regeneration ability of FPHA. According to the histological analysis results, the blank group also showed extensive new bone formation, which was due to the characteristics of the acute buccal bone defect model. At the early stage of healing, a certain amount of new bone formation always occurs in fresh bone defects regardless of whether bone substitutes are grafted [32, 33]. However, the ridge contour in the blank group was significantly collapsed compared with that in the bone substitute groups due to the insufficient supporting capacity of the CMs alone. Osteogenesis is a slow and gradual process, and the main differences between grafted and non-grafted bone substitute sites are the space maintenance capacity and long-term efficacy. Generally, new bone forms gradually from the parent bone region to the center of the defect area, similar to the biological process of the GBR procedure [34], because the pre-osteoblastic cells, osteogenic factors, and blood supply for bone regeneration are all provided by the parent bone. In the present study, the NB adjacent to the border of the parent bone was obviously more mature than the new bone far from the parent bone, confirming that the direction of new bone formation was from the parent bone to the central region of the defect area. Furthermore, more lamellar bone was adjacent to the parent bone, whereas more woven bone was found in the central regions of the defects. These findings are consistent with the basic concept of bone healing and remodeling [35, 36]. In the ROIs of both the PHA and FPHA groups, a small amount of woven bone was observed around the mature bone, and a few multinucleated osteoclast-like cells were attached onto the demineralized surfaces of the material particles, indicating that bone remodeling was still active at 12 weeks after bone augmentation. Bone substitutes, together with NB, blood vessels and osteogenic-associated cells, form a microenvironment contributing to bone regeneration. Woven bone and blood vessels could also be identified inside the macropores of the PHA and FPHA particles, suggesting the prominent osteoconductivity of the material. Material particles were found to be more concentrated adjacent to the BD, which may be explained by gravity and the dogs' daily feeding.

Macroscopically, the DH and ridge width measurements at different height levels of the ROI demonstrated that PHA and FPHA bone graft materials can substantially support the contour of the alveolar ridge and maintain the vertical height to a certain extent. Moreover, the ridge width maintenance capacity of FPHA was significantly superior to that of PHA at the middle third of the DH. This more reliable contour-preserving capacity might be due to the enhanced compressive strength of PHA after fluorine substitution. Compressive strength is considered one of the most critical physical properties of bone substitutes and influences the outcome of bone augmentation, especially in load-bearing areas [6, 7]. The mechanical behavior of porcine bone was reported to be more similar to that of human bone rather than bone tissue derived from other origins [37]. However, during the preparation of PHA, calcination greatly reduced its mechanical strength, which may increase the risk of its use for bone augmentation in load-bearing areas. Fluoride incorporation has been reported to potentially alter the crystal structure and increase the densification behavior of HA, improving its mechanical strength [38]. In our previous study, we demonstrated that a certain amount of fluorination can increase the compressive strength of PHA to 4- to 6-times the original strength [15]. In the present study, both FPHA and PHA were applied to repair buccal bone defects in canine mandibles. Pressure at the bone augmentation sites was inevitable, although a soft-food diet was adopted for the canines. Therefore, the increase in compressive strength described above may further contribute to the enhanced mechanical performance of FPHA, which may explain why the FPHA-grafted sites showed a superior ridge width maintenance capacity compared with the PHA-grafted sites.

After 12 weeks of healing, the PHA and FPHA groups showed comparable proportions of residual bone graft materials. Relatively intact bone graft material particles were observed in all PHA and FPHA samples, with no significant signs of particle breakage or absorption. In the histological sections, biodegradation of graft materials mediated by osteoclasts or multinucleated giant cells could only be identified occasionally. The in vivo degradation of most biological HAs, including PHA, is very slow [39, 40]. Previous studies demonstrated that HA in the bone graft area could only be engulfed as a foreign body by macrophages; however, biological HA, such as PHA and FPHA, is biocompatible and shows only weak immunogenicity [15, 16]. Without further inflammation after implantation in the bone graft sites, PHA and FPHA showed very slow biodegradation in the present study. Therefore, both the PHA and FPHA bone graft materials can offer a predictable augmented space maintenance capacity and ensure the long-term stability of the bone augmentation area.

A large number of experimental animal studies have evaluated the bone augmentation efficiency of bone substitutes using the GBR technique, but the study parameters, such as the test animals (rats, rabbits, minipigs, dogs, monkeys), the types and sizes of bone defects (acute, chronic, transosseous, contained) and the defect locations (ramus, alveolar ridge), are variable [37, 41]. The present study applied a canine model to establish acute, non-contained osseous defects in the mandible to evaluate a new bone substitute material. This experimental model was selected according to the surgical procedure reported in previous studies employing the same model [42, 43]. In all these studies, the bone defects were surgically created in edentulous mandibles using the same surgical procedure with lateral bone augmentation, where the lack of buccal bone walls presented a challenge for re-establishing the original morphology and dimension of the ridge. An acute-type buccal bone defect is designed to simulate immediate grafting of a bone substitute to a fresh bone defect after tooth extraction or dental trauma in clinical practice, whereas a chronic-type buccal bone defect model simulates chronic atrophy of the alveolar ridge after tooth extraction, which is a more common clinical condition [41, 44, 45]. However, shaping the graft material would be difficult because the border of the defect area is indistinct, and the grafted particles are hardly contained in the chronic bone defect. Therefore, acute bone defects are beneficial for standardizing the sizes of defect areas and are easy to establish.

The results of the present study showed the superiority of the space maintenance capacity and osteoconductivity of a novel FPHA as a bone graft material in canine mandible defects. However, certain limitations should be noted. Normalizing the size of a bone defect is easy with a standard acute bone defect model, but such model fails to simulate the clinical condition of buccal atrophy of the alveolar ridge, which gradually forms after tooth extraction. Therefore, more types of animal models should be introduced in future studies. FPHA is expected to be applied as a bone substitute in dental implant-related bone augmentation surgery; thus, the interaction between FPHA and the implant surface must also be explored in future studies. In this study, only one end point was designed to evaluate the bone regeneration capacity of the materials. To comprehensively understand the bone remodeling process of the bone graft materials, more time periods, including the early, middle and late stages, are necessary for further investigations.

Conclusions

FPHA can be prepared from porcine bone by incorporating fluoride ions via simple chemical and thermal treatments. Within the limits of this animal study, FPHA particles covered with CMs were found to be superior to PHA particles grafted using the same procedure in terms of ridge width maintenance and new bone formation. Therefore, fluorine incorporation is an effective method to enhance the bone regeneration capacity of PHA.

Acknowledgements

This work was financially supported by the National Natural Science Foundation of China (81600914, 81970975), the Guangdong Natural Science Foundation of China (2016A030310173, 2017A030310207) and the Guangdong Financial Fund for High-Caliber Hospital Construction (174-2018-XMZC-0001-03-0125/D-10).

Disclosure of conflict of interest

None.

Address correspondence to: Drs. Zhipeng Li and Zhuofan Chen, Guanghua School of Stomatology, Hospital of Stomatology, Sun Yat-sen University, No. 56, Lingyuan West Road, Guangzhou 510060, China. Tel: +86-020-83862537; Fax: +86-020-83822807; E-mail: implants@163.com (ZPL); chzhuof@mail.sysu.edu.cn (ZFC)

References

[1] Araujo MG and Lindhe J. Dimensional ridge alterations following tooth extraction. An experimental study in the dog. J Clin Periodontol 2005; 32: 212-218.

[2] Vignoletti F, Discepoli N, Muller A, Sanctis M, Munoz F and Sanz M. Bone modelling at fresh extraction sockets: immediate implant placement versus spontaneous healing. An experimental study in the beagle dog. J Clin Periodontol 2012; 39: 91-97.

[3] Buser D, Dula K, Lang NP and Nyman S. Long-term stability of osseointegrated implants in bone regenerated with the membrane technique. 5-year results of a prospective study with 12 implants. Clin Oral Implants Res 1996; 7: 175-183.

[4] Benic GI and Hämmerle CH. Horizontal bone augmentation by means of guided bone regeneration. Periodontol 2000 2014; 66: 13-40.

[5] Retzepi M and Donos N. Guided Bone Regeneration: biological principle and therapeutic applications. Clin Oral Implants Res 2010; 21: 567-576.

[6] Ito K, Yamada Y, Nagasaka T, Baba S and Ueda M. Osteogenic potential of injectable tissue-engineered bone: a comparison among autogenous bone, bone substitute (Bio-oss), platelet-rich plasma, and tissue-engineered bone with respect to their mechanical properties and histological findings. J Biomed Mater Res A 2005; 73: 63-72.

[7] Hannink G and Arts JJ. Bioresorbability, porosity and mechanical strength of bone substitutes: what is optimal for bone regeneration? Injury 2011; 42: S22-S25.

[8] Kolk A, Handschel J, Drescher W, Rothamel D, Kloss F, Blessmann M, Heiland M, Wolff KD and Smeets R. Current trends and future perspectives of bone substitute materials - from space holders to innovative biomaterials. J Craniomaxillofac Surg 2012; 40: 706-718.

[9] Bohner M, Galea L and Doebelin N. Calcium phosphate bone graft substitutes: failures and hopes. J Eur Ceram Soc 2012; 32: 2663-2671.

[10] Fox K, Tran PA and Tran N. Recent advances in research applications of nanophase hydroxyapatite. Chemphyschem 2012; 13: 2495-2506.

[11] Liu Q, Huang SS, Matinlinna JP, Chen ZF and Pan HB. Insight into biological apatite: physiochemical properties and preparation approaches. Biomed Res Int 2013; 2013: 1-13.

[12] Boutinguiza M, Pou J, Comesana R, Lusquinos F, de Carlos A and Leon B. Biological hydroxyapatite obtained from fish bones. Mater Sci Eng C Mater Biol Appl 2012; 32: 478-486.

[13] Liu Q, Chen ZT, Gu HJ and Chen ZF. Preparation and characterization of fluorinated porcine hydroxyapatite. Dent Mater J 2012; 31: 742-750.

[14] Li ZP, Huang BX, Mai S, Wu XY, Zhang HQ, Qiao W, Luo X and Chen ZF. Effects of fluoridation of porcine hydroxyapatite on osteoblastic activity of human MG63 cells. Sci Technol Adv Mater 2015; 16: 1-11.

[15] Qiao W, Liu Q, Li ZP, Zhang HQ and Chen ZF. Changes in physicochemical and biological properties of porcine bone derived hydroxyapatite induced by the incorporation of fluoride. Sci Technol Adv Mater 2017; 18: 110-121.

[16] Liu RH, Qiao W, Huang BX, Chen ZT, Fang JH, Li ZP and Chen ZF. Fluorination enhances the osteogenic capacity of porcine hydroxyapatite. Tissue Eng Part A 2018; 24: 1207-1217.

[17] Yamaguchi M and Weitzmann MN. Zinc stimulates osteoblastogenesis and suppresses osteoclastogenesis by antagonizing NF-kappa B activation. Mol Cell Biochem 2011; 355: 179-186.

[18] Saidak Z and Marie PJ. Strontium signaling: molecular mechanisms and therapeutic implications in osteoporosis. Pharmacol Ther 2012; 136: 216-226.

[19] Li H and Chang J. Bioactive silicate materials stimulate angiogenesis in fibroblast and endothelial cell co-culture system through paracrine effect. Acta Biomater 2013; 9: 6981-6991.

[20] Shao HF, Liu A, Ke XR, Sun M, He Y, Yang XY, Fu JZ, Zhang L, Yang GJ, Liu YM, Xu SZ and Gou ZR. 3D robocasting magnesium-doped wollastonite/TCP bioceramic scaffolds with improved bone regeneration capacity in critical sized calvarial defects. J Mater Chem B 2017; 5: 2941-2951.

[21] Wang YS, Zhang S, Zeng XT, Ma LL, Weng WJ, Yan WQ and Qian M. Osteoblastic cell response on fluoridated hydroxyapatite coatings. Acta Biomater 2007; 3: 191-197.

[22] Ohno M, Kimoto K, Toyoda T, Kawata K and Arakawa H. Fluoride-treated bio-resorbable synthetic hydroxyapatite promotes proliferation and differentiation of human osteoblastic MG-63 cells. J Oral Implantol 2013; 39: 154-160.

[23] Yao F and LeGeros RZ. Carbonate and fluoride incorporation in synthetic apatites: comparative effect on physico-chemical properties and in vitro bioactivity in fetal bovine serum. Mater Sci Eng C Mater Biol Appl 2010; 30: 423-430.
[24] Park SA, Shin JW, Yang YI, Kim YK, Park KD, Lee JW, Jo IH and Kim YJ. In vitro study of osteogenic differentiation of bone marrow stromal cells on heat-treated porcine trabecular bone blocks. Biomaterials 2004; 25: 527-535.
[25] Qu X, Wan YQ, Zhang HW, Cui WJ, Bei JZ and Wang SG. Porcine-derived xenogeneic bone/poly(glycolide-co-lactide-co-caprolactone) composite and its affinity with rat OCT-1 osteoblast-like cells. Biomaterials 2006; 27: 216-225.
[26] Qiao W, Liu R, Li Z, Luo X, Huang B, Liu Q, Chen Z, Tsoi JKH, Su YX, Cheung KMC, Matinlinna JP, Yeung KWK and Chen Z. Contribution of the in situ release of endogenous cations from xenograft bone driven by fluoride incorporation toward enhanced bone regeneration. Biomater Sci 2018; 6: 2951-2964.
[27] Kannan S, Rocha JH, Agathopoulos S and Ferreira JM. Fluorine-substituted hydroxyapatite scaffolds hydrothermally grown from aragonitic cuttlefish bones. Acta Biomater 2007; 3: 243-249.
[28] Sun Y, Wang CY, Wang ZY, Cui Y, Qiu ZY, Song TX and Cui FZ. Test in canine extraction site preservations by using mineralized collagen plug with or without membrane. J Biomater Appl 2016; 30: 1285-1299.
[29] Wang YF, Wang CY, Wan P, Wang SG and Wang XM. Comparison of bone regeneration in alveolar bone of dogs on mineralized collagen grafts with two composition ratios of nano-hydroxyapatite and collagen. Regen Biomater 2016; 3: 33-40.
[30] Hsu JT, Chen YJ, Ho JT, Huang HL, Wang SP, Cheng FC, Wu J and Tsai MT. A comparison of micro-CT and dental CT in assessing cortical bone morphology and trabecular bone microarchitecture. PLoS One 2014; 9: 1-8.
[31] Lv HC, Zhang LC, Yang F, Zhao Z, Yao Q, Zhang LH and Tang PF. Comparison of microstructural and mechanical properties of trabeculae in femoral head from osteoporosis patients with and without cartilage lesions: a case-control study. BMC Musculoskelet Disord 2015; 16: 1-10.
[32] Strietzel FP, Khongkhunthian P, Khattiya R, Patchanee P and Reichart PA. Healing pattern of bone defects covered by different membrane types - a histologic study in the porcine mandible. J Biomed Mater Res B Appl Biomater 2006; 78: 35-46.
[33] De Angelis N, Felice P, Pellegrino G, Camurati A, Gambino P and Esposito M. Guided bone regeneration with and without a bone substitute at single post-extractive implants: 1-year post-loading results from a pragmatic multicentre randomised controlled trial. Eur J Oral Implantol 2011; 4: 313-325.
[34] Elgali I, Turri A, Xia W, Norlindh B, Johansson A, Dahlin C, Thomsen P and Omar O. Guided bone regeneration using resorbable membrane and different bone substitutes: early histological and molecular events. Acta Biomater 2016; 29: 409-423.
[35] Dahlin C, Linde A, Gottlow J and Nyman S. Healing of bone defects by guided tissue regeneration. Plast Reconstr Surg 1988; 81: 672-676.
[36] Dominiak M, Lysiak-Drwal K, Gedrange T, Zietek M and Gerber H. Efficacy of healing process of bone defects after apectomy: results after 6 and 12 months. J Physiol Pharmacol 2009; 60: 51-55.
[37] Pearce AI, Richards RG, Milz S, Schneider E and Pearce SG. Animal models for implant biomaterial research in bone: a review. Eur Cell Mater 2007; 13: 1-10.
[38] Bianco A, Cacciotti I, Lombardi M, Montanaro L, Bemporad E and Sebastiani M. F-substituted hydroxyapatite nanopowders: thermal stability, sintering behaviour and mechanical properties. Ceram Int 2010; 36: 313-322.
[39] Crespi R, Cappare P and Gherlone E. Comparison of magnesium-enriched hydroxyapatite and porcine bone in human extraction socket healing: a histologic and histomorphometric evaluation. Int J Oral Maxillofac Implants 2011; 26: 1057-1062.
[40] Zhao HS, Wang GC, Hu SP, Cui JJ, Ren N, Liu D, Liu HB, Cao CB, Wang JY and Wang ZL. In vitro biomimetic construction of hydroxyapatite-porcine acellular dermal matrix composite scaffold for MC3T3-E1 preosteoblast culture. Tissue Eng Part A 2011; 17: 765-776.
[41] von Arx T, Cochran DL, Hermann JS, Schenk RK and Buser D. Lateral ridge augmentation using different bone fillers and barrier membrane application - a histologic and histomorphometric pilot study in the canine mandible. Clin Oral Implants Res 2001; 12: 260-269.
[42] Vierra M, Mau LP, Huynh-Ba G, Schoolfield J and Cochran DL. A lateral ridge augmentation study to evaluate a synthetic membrane for guided bone regeneration: an experiment in the canine mandible. Clin Oral Implants Res 2016; 27: 73-82.
[43] Lee KS, Jeon YS, Shin SW and Lee JY. Effects of rhBMP-2 loaded titanium reinforced collagen membranes on horizontal bone augmentation in dogs. Biomed Res Int 2017; 2017: 1-8.
[44] Schwarz F, Ferrari D, Balic E, Buser D, Becker J and Sager M. Lateral ridge augmentation us-

ing equine- and bovine-derived cancellous bone blocks: a feasibility study in dogs. Clin Oral Implants Res 2010; 21: 904-912.

[45] Sanz M, Ferrantino L, Vignoletti F, de Sanctis M and Berglundh T. Guided bone regeneration of non-contained mandibular buccal bone defects using deproteinized bovine bone mineral and a collagen membrane: an experimental in vivo investigation. Clin Oral Implants Res 2017; 28: 1466-1476.